Local Control of Neurofilament Accumulation during Radial Growth of Myelinating Axons In Vivo: Selective Role of Site-specific Phosphorylation

Ivelisse Sánchez,*‡ Linda Hassinger,‡ Ram K. Sihag,‡ Don W. Cleveland,‖ Panaiyur Mohan,‡ and Ralph A. Nixon*‡§

*Department of Psychiatry and §Program in Neuroscience, Harvard Medical School, Boston, Massachusetts 02115; ‡Laboratories for Molecular Neuroscience, McLean Hospital, Belmont, Massachusetts; and ‖Ludwig Cancer Institute at University of California at San Diego, La Jolla, California 92093

Abstract. The accumulation of neurofilaments required for postnatal radial growth of myelinated axons is controlled regionally along axons by oligodendroglia. Developmentally regulated processes previously suspected of modulating neurofilament number, including heavy neurofilament subunit (NFH) expression, attainment of mature neurofilament subunit stoichiometry, and expansion of interneurofilament spacing cannot be primary determinants of regional accumulation as we show each of these factors precede accumulation by days or weeks. Rather, we find that regional neurofilament accumulation is selectively associated with phosphorylation of a subset of Lys-Ser-Pro (KSP) motifs on heavy neurofilament subunits and medium-size neurofilament subunits (NFMs), rising >50-fold selectively in the expanding portions of optic axons. In mice de-

leted in NFH, substantial preservation of regional neurofilament accumulation was accompanied by increased levels of the same phosphorylated KSP epitope on NFM. Interruption of oligodendroglial signaling to axons in Shiverer mutant mice, which selectively inhibited this site-specific phosphorylation, reduced regional neurofilament accumulation without affecting other neurofilament properties or aspects of NFH phosphorylation. We conclude that phosphorylation of a specific KSP motif triggered by glia is a key aspect of the regulation of neurofilament number in axons during axonal radial growth.

Key words: axon caliber • axon–glia interactions • oligodendroglia • CNS development • protein phosphorylation

Introduction

After reaching their synaptic targets, axons expand up to 3–10-fold to achieve the large diameters required for the rapid conduction of action potentials (Goldberg and Frank, 1979; Graf von Keyserlingk and Schramm, 1984). Expansion is triggered locally when a portion of the axon is wrapped by oligodendrocyte or Schwann cell processes before the elaboration of myelin (Sanchez et al., 1996). Portions of axons or entire axons that remain unmyelinated do not expand (Colello et al., 1994; Nixon et al., 1994). Associated with the process of axon radial growth is a local accumulation of neurofilaments within the expand-

ing region. These 10-nm neuronal intermediate filaments are composed of three subunits designated heavy, medium, and light (NFH,[1] NFM, and NFL, respectively) according to their respective molecular masses. The requirement for neurofilaments to achieve mature axonal caliber has been clearly demonstrated (Ohara et al., 1993; Eyer and Peterson, 1994), but the mechanisms regulating neurofilament accumulation are unknown.

Neurofilament number within axons is influenced by several factors. After axons make synaptic contacts, the synthesis of neurofilament subunits and other cytoskeletal proteins increases and the rates of slow axonal transport of these proteins decrease severalfold (Hoffman et al., 1983; Willard and Simon, 1983). These changes may raise the levels of many cytoskeletal proteins along the entire length of the axon, but they do not account for the selective expansion of myelinating axonal regions, which

[1]*Abbreviations used in this paper:* CNS, central nervous system; ddw, double distilled water; ERK, extracellular signal–regulated kinase; KSP, Lys-Ser-Pro; MBP, myelin basic protein; NFH, heavy neurofilament subunit; NFL, light neurofilament subunit; NFM, medium-size neurofilament subunit; RGC, retinal ganglion cell; TBS, Tris-buffered saline.

achieve diameters and numbers of neurofilaments that may be manyfold larger than those in an immediately adjacent unmyelinated region. Developmentally regulated properties of neurofilaments that might mediate neurofilament accumulation selectively within a discrete region of an axon include the state of phosphorylation and subunit composition as considered briefly below.

During early postnatal development, the COOH-terminal side arm domains of NFH and NFM subunits become extensively phosphorylated within a multiphosphorylation repeat (MPR) region containing the sequence motif Lys-Ser-Pro (KSP) (Carden et al., 1987; Clark and Lee, 1991). In the case of NFH, the >40 KSP repeats present in this region can be separated into two categories, KSPXX and KSPXK (where the final X is any amino acid except lysine), which are believed to be regulated by different protein kinases (Bennett et al., 1994; Elhanany et al., 1994). Several studies suggest that, among numerous candidate neurofilament protein kinases (115 kD, glycogen synthetic kinase [GSK] 3, extracellular signal–regulated kinase [ERK], stress-activated protein kinase, protein kinase K, protein kinase C), Cdk-5 preferentially phosphorylates the KSPXK repeats (Hisanaga et al., 1993; Shetty et al., 1993; Guidato et al., 1996; Sun et al., 1996) and has been reported to generate epitopes recognized by the monoclonal antibodies SMI31 and RT97 (Bajaj and Miller, 1997). In contrast, ERKs and GSK appear to regulate KSPXX repeats and generate the SMI34 as well as SMI31 epitopes (Roder and Ingram, 1991; Pant and Veeranna, 1995). Phosphorylation at the COOH-terminal domains of NFH and NFM in vitro straightens individual neurofilaments and promotes their alignment into bundles (Leterrier et al., 1996) and, in vivo, is associated with an increased interneurofilament spacing (Hsieh et al., 1994; Nixon et al., 1994), as NFH and NFM COOH-terminal side arms extend and form crossbridges among neurofilaments and other cytoskeletal elements (Hirokawa et al., 1984; Gotow and Tanaka, 1994; Gotow et al., 1994). Neurofilament transport slows when NFH and NFM are extensively phosphorylated (Watson et al., 1989; Archer et al., 1994). When these subunits are at their highest states of phosphorylation, neurofilaments may stop moving for extremely long periods of time (Lewis and Nixon, 1988), presumably reflecting their integration within a stationary but dynamic cytoskeletal network along axons (for reviews see Hirokawa et al., 1984; Nixon, 1998a,b). Although it is likely that the different properties and behaviors of neurofilaments within axons are independently regulated by the phosphorylation of specific sites within the MPR domain, this possibility has not been previously addressed.

The subunit composition of neurofilaments also influences neurofilament number in axons under some conditions (Cote et al., 1993; Collard et al., 1995; Wong et al., 1995; Xu et al., 1996). The delayed expression of NFH during development occurs during the same period as when slow axonal transport rates decrease and neurofilament levels within axons increase (Hoffman et al., 1983; Willard and Simon, 1983). Moreover, increasing the NFH content of neurofilaments by overexpressing NFH in transgenic mice slows neurofilament transport and raises axonal levels of neurofilaments proximally along axons (Cote et al., 1993; Collard et al., 1995; Marszalek et al., 1996). In both of these situations, the potential contribution of subunit phosphorylation to these effects is unclear. More recently, targeted disruption of neurofilament subunit genes (Elder et al., 1998a; Rao et al., 1998; Zhu et al., 1998) has been used to investigate the roles of each neurofilament subunit in axon radial growth. Ablation of the genes for either NFM or NFL significantly reduced neurofilament numbers and axonal calibers (Ohara et al., 1993; Zhu et al., 1997; Elder et al., 1998a). Neurofilament assembly requires NFL (Ching and Liem, 1993; Lee et al., 1993), and the markedly lowered NFL levels in NFM-deleted mice (Elder et al., 1998b) presumably accounts in part for reduced axon calibers in these mice. Mice lacking NFH have also been generated (Elder et al., 1998b; Rao et al., 1998; Zhu et al., 1998). The small though appreciable effects of this gene deletion on motor axon caliber led some investigators to question the role of NFH in determining axon caliber and, by inference, regulating neurofilament number. However, revealing the function of a protein based solely on the magnitude of phenotypic changes after gene ablation may be problematic because functions of the deleted protein are often compensated by other proteins. In this regard, modest caliber reductions were observed in NFH-deleted mice, but effects of NFH deletion were partially compensated by increases in NFM levels and numbers of microtubules (Rao et al., 1998; Zhu et al., 1998).

To distinguish the roles of subunit stoichiometry and phosphorylation as determinants of regional neurofilament accumulation, we characterized the changes in molecular and structural properties of neurofilaments as they occurred differentially in expanding and unexpanded portions of mouse optic axons during development. We combined analyses of normal retinal ganglion cell development with specific perturbations of neurofilament behavior in NFH-deleted mice and in Shiverer (Shi) mutant mice carrying a mutation of the myelin basic protein (MBP) gene, which interferes with oligodendrocyte maturation (Chernoff, 1981; Shine et al., 1992) and prevents most axons from receiving signals that trigger regional neurofilament accumulation (Sanchez et al., 1996). Our results show that the regional neurofilament accumulation associated with the greatest radial growth of axons begins well after neurofilament subunits achieve mature stoichiometry and, instead, is closely related to the phosphorylation of a subset of KSP sites on the NFH COOH terminus. In the absence of NFH, NFM partially assumes the role of this phosphorylation event during regional neurofilament accumulation.

Materials and Methods

Animals

Breeding of the C57BL/6J mice and tissue dissections were performed as described previously (Nixon and Lewis, 1986; Sanchez et al., 1996) using mice at six postnatal ages (9–120 d). Production of NFH null mice is described (Rao et al., 1998); mice 1.5 yr of age were used.

Electron Microscopy

Mice were anesthetized with halothane gas and the tissue was fixed through intracardial perfusion with 4% paraformaldehyde, 5% glutaraldehyde in 0.1 M PBS, pH 7.4, at room temperature. The optic nerve was dissected and processed as described by Nixon et al. (1994), segmented in 1.2-mm pieces, cleared in propylene oxide, and embedded in Medcast

(Ted Pella, Inc.). Ultrathin sections were collected and the section containing the initial portion of the retinal excavation was then used as a standard reference point. Ultrathin sections were stained with uranyl acetate and lead citrate and examined in a EX electron microscope (model JEM1200; JEOL) at 80 kV.

Immunoelectron Microscopy

Thin sections of epon-embedded tissue were picked up on formvar-coated nickel grids. These sections were etched with 1% periodic acid for 10 min, rinsed in double distilled water (ddw), etched with 3% sodium metaperiodate for 30 min, and rinsed in ddw, followed by 0.05 M Tris-buffered saline (TBS), pH 7.6, for 5 min. Sections were then blocked with 20% normal goat serum in TBS for 60 min at room temperature and then incubated overnight at room temperature in a moist chamber with primary antibody (RT97) diluted at 1:5,000 in TBS containing 1% normal goat serum, 1% BSA, and 0.1% Triton X-100. The sections were washed sequentially in TBS, pH 7.6, for 5 min, in TBS, pH 8.2, for 5 min, and in TBS, pH 8.2, with 0.5% polyethylene glycol for 5 min. Sections were then incubated in 5-nm gold conjugate IgG diluted to 1:25 in TBS containing polyethylene glycol, pH 8.2, for 2 h at room temperature, followed by rinses, first in TBS then in ddw. Finally, the sections were counterstained in uranyl acetate and lead citrate and examined with an EX microscope (model JEM1200; JEOL) with an AMT digital camera.

Determination of Axonal Diameter Sizes and Quantitation of Neurofilaments

Axonal diameters were determined from 1,561–4,919 axons at the 50- and 700-μm levels from each of the six postnatal ages analyzed (P9, 12, 16, 21, 30, and 120) and from NFH-deleted and control mice aged 1.5–1.7 yr old. Neurofilament and microtubule numbers in each optic nerve were determined from electron micrographs at the 50- and 700-μm levels by counting 600–1,185 axon profiles representative of the range in calibers in the total axonal population to accurately reflect absolute numbers of neurofilaments in a population of axons heterogeneous in caliber. Values were expressed as number of neurofilaments per 1,000 axons as described previously (Sanchez et al., 1996).

SDS-PAGE, Immunoblotting, and Two-dimensional Gel Electrophoresis

The most proximal 2.2-mm segment of the optic nerve from C57Bl/6J mice at postnatal ages of 4 d through adult (120 d) was removed at 4°C after mice were killed by cervical dislocation. Segments from eight mice of a given age were pooled and stored at −70°C. The optic nerve cytoskeleton proteins were obtained from pooled segments for each given age. All subunit levels in developing mice were measured based on the standard optic nerve length. In studies of adult NFH-null and Shiverer mice, we used the standard 9-mm length of optic pathway used in previous studies (Nixon and Logvinenko, 1986), which extended from the eye to the optic tract. The tissue was homogenized as shown by Chiu and Norton (1982) with 50 mM Tris-HCl, pH 6.8, buffer containing 1% Triton, 50 mM NaF, 5 mM NaVO$_3$, 10 μm genistein, 0.25 M NaCl, 50 μg/ml leupeptin, 0.1% aprotinin, and 2 mM PMSF (buffer A). The homogenate was centrifuged at 15,000 g for 10 min at 4°C and the pellet and supernatant were separated and processed immediately. Equal aliquots of Triton-insoluble fractions pooled from the 2.2-mm proximal segments as described were loaded onto each lane. Protein separation was accomplished by gel electrophoresis, as described by Laemmli (1970), with the use of 10% polyacrylamide gels and a Hoefer minigel format for most experiments. Proteins were transferred to nitrocellulose membranes as described by Towbin et al. (1979), except for the inclusion of 0.1% SDS and the omission of methanol in the transfer buffer. Nonfat milk (5%) in TBS with 0.3% Tween was used to block nonspecific antibody binding. Total levels of NFH protein were determined using the antibody SMI33, which recognizes NFH and NFM, irrespective of their phosphorylation states. Varying states of phosphorylation on the COOH terminus of NFH were detected using the phosphorylation-dependent antibodies SMI31, SMI34, and RT97 (Sternberger and Sternberger, 1983; Coleman and Anderton, 1990). Immunostaining was performed using HRP-labeled anti–rabbit or anti–mouse biotinylated antibodies and a DAB chromogen as described by the manufacturer (Vector Laboratories). NFH levels in the Triton-insoluble and -soluble protein fractions were qualitatively determined by using the ECL chemiluminescence developing system (Amersham Pharmacia Biotech). Immunoreactivity levels were quantified by analyzing digitized im-

ages generated by the Ofoto program (Light Source, Inc.) with Scan Analysis® software (Specom Research). Quantitations were performed within the linear range of the densitomer. A standard curve for each antibody was derived from subsequent dilutions of adult neurofilament protein immunoblotted and stained with the respective antibodies. Immunoreactivity levels were expressed relative to the value at P120 for each antibody separately. The data were plotted using a linear scale on the x-axis. Two-dimensional electrophoresis (3.5–9 pH range) was performed according to O'Farrell (1975), using the Hoefer 460 system.

Confocal Immunofluorescence Microscopy

C57Bl/6J mice were anesthetized with haloethane gas and perfused intracardially with 4% paraformaldehyde in PBS, pH 7.4. Retina whole mounts were stained with a cocktail of N-52 (Sigma-Aldrich) and SMI32 (Sternberger Monoclonal) anti-NFH antibodies to recognize all forms of NFH. The immunoreactivity was visualized with a 410 LSM Laser Confocal system (ZEISS) after staining with fluorescein labeled anti–mouse antibody (Vector Laboratories).

Proteolytic Digestion and HPLC Separation of NFH Peptides

The mouse spinal cord cytoskeleton was prepared in the presence of phosphatase and protease inhibitors as described previously (Sihag and Nixon, 1989) and the proteins were separated on 24-cm-long 6% SDS-polyacrylamide gels. The 200-kD polypeptide band identified as NFH was excised from gel, and the gel slices were washed extensively with 20% methanol. The gel slices were lyophilized and homogenized and the NFH polypeptide was digested with 2 μg/ml TPCK-trypsin or TLCK-α-chymotrypsin in 50 mM NH$_4$HCO$_3$ for 20 h at 37°C. The proteolytic reactions were inhibited by addition of 10 μg/ml of AEBSF, 10 μg/ml aprotinin, and 2 mM PMSF. The resulting NFH peptides were lyophilized, solubilized in a 20% acetic acid and 5% formic acid solution, and separated on a preparative C18 reverse-phase HPLC column as described previously (Sihag and Nixon, 1989). The 2–80% acetonitrile gradient was run in 45 min and 1-ml/min fractions were collected. The HPLC fractions from 3 to 30 containing the tryptic or TLCK-α-chymotrypsin NFH peptides were lyophilized, solubilized in 50 mM NH$_4$HCO$_3$, and either dot-blotted on a 0.22-μm PVDF membrane or pooled to be further affinity-purified, respectively. Immunoreactivity of the dot-blotted peptides was examined with SMI34, SMI31, or RT97.

Affinity Purification of RT97 and SMI31 Immunoreactive Peptides

Cyanobromide-activated Sepharose 4B (BD PharMingen) was coupled to protein A–purified RT97 or to SMI31 antibodies using the protocol recommended by the manufacturer, and the slurry was poured into 1-ml syringe columns. The tryptic and chymotryptic digests of NFH were prepared as described above. Equal aliquots of the digest were passed thrice through the RT97 or SMI31 affinity columns. The unbound peptides were removed by several washes with 10 volumes of TBS. The NFH peptides that bound to the RT97 or SMI31 affinity columns were eluted with 0.1 M glycine, pH 2.7, and neutralized with 1 M Tris-HCl, pH 8.0. The column fractions were then analyzed by dot blot on PVDF membranes. The immunoreactivity of the eluted peptides from each column was tested against both RT97 and SMI31 by using the ECL development system (Amersham Pharmacia Biotech).

Results

Oligodendroglial-triggered Axon Caliber Expansion Coincides with Regional Accumulation of Neurofilaments

Axons of retinal ganglion cells are unmyelinated within the retina and for a distance of ∼100 μm after they converge at the retinal excavation to form the optic nerve (Fig. 1, A and B). Beyond the lamina cribrosa, which is a specialized meshwork of astrocytes located at 100–150 μm from the retinal excavation, >95% of the axons in adult mice are myelinated, larger in caliber, and contain more
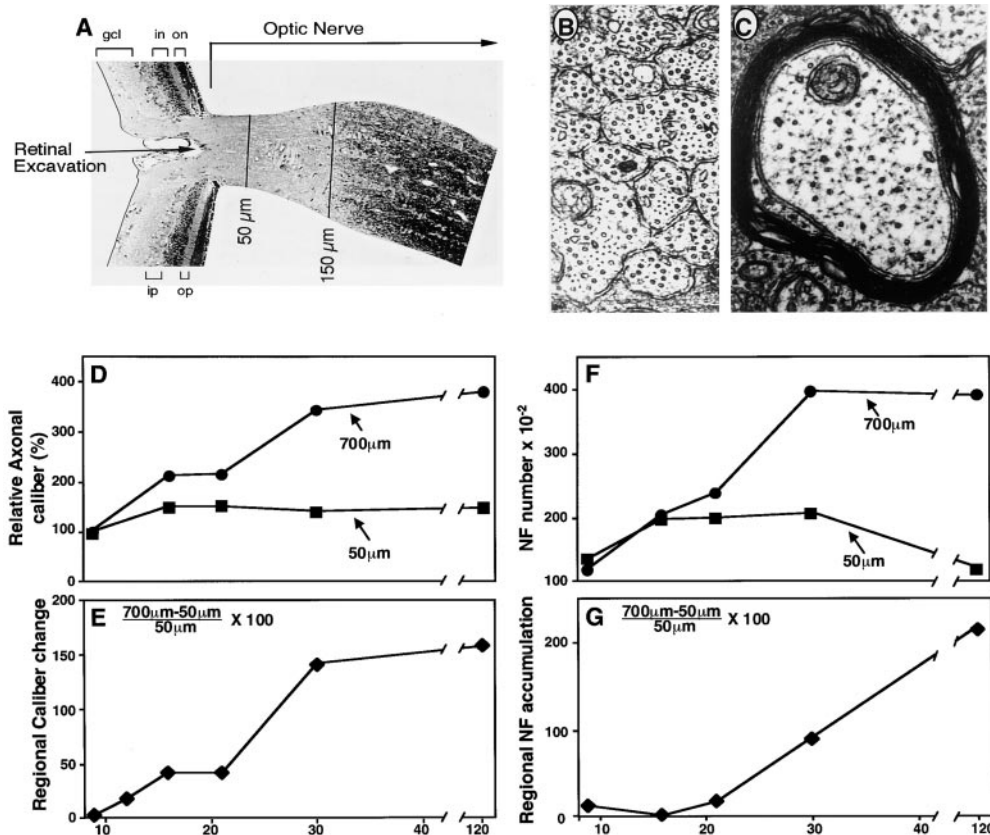
Figure 1. Regional changes in axon caliber and neurofilament distribution. (A) Toluidine blue–stained sagittal section through the retina and proximal optic nerve of the adult mouse reveals the retinal ganglion cell layer (gcl), inner plexiform (ip), inner nuclear (in), outer plexiform layer (op), and outer nuclear layer (on) of the retina. Ultrastructure of two regions of the optic nerve from a 21-d-old mouse located 50 μm (B) or 700 μm (C) from the retinal excavation. Relative average axonal cross-sectional areas at the 50- and 700-μm levels (D) for representative subpopulations of the total axonal population were measured from electron micrographs (Sanchez et al., 1996). A total of 17,000 axons were analyzed. (E) The percent increase in axonal cross-sectional area at the 700-μm level over the area at the 50-μm level (i.e., [700 − 50 μm/50 μm] × 100), referred to as "regional caliber change," is plotted as a function of postnatal age. (F) The absolute numbers of neurofilaments at 50-μm (■) and 700-μm (●) levels of the optic nerve in 2–3 mice were determined at different postnatal ages in 300–555 axons of calibers representative of the total optic axon population. Interanimal variation <5%. Values are displayed as total neurofilament number per 1,000 axons at each age. (G) To emphasize the regional accumulation of neurofilaments along the axons, the percentage increase in neurofilament number at the 700-μm level over the number at the 50-μm level (i.e., [700 μm − 50 μm/50 μm] × 100) for each postnatal age is plotted.

neurofilaments (Fig. 1, A and C) (Nixon et al., 1994). During postnatal development, the cross-sectional areas of optic axons at levels beyond the lamina cribrosa increase an additional 200% under the control of signals from oligodendroglial cells (Sanchez et al., 1996). Our results showed that >80% of the total regional caliber growth occurred between 21 and 30 d postnatally (Fig. 1, D and E). Regional caliber expansion is defined as the percent increase in the axonal cross-sectional area at the 700-μm level (or more distal levels) over the area at a level 50 μm (Fig. 1 E) from the retinal excavation (i.e., Area [700 μm − 50 μm/50 μm] × 100).

Before postnatal day 16, neurofilaments increased modestly in number at axonal levels both proximal and distal to the lamina cribrosa without resulting in a regional differential of neurofilaments along these axons (Fig. 1, F and G). After P21, however, neurofilaments robustly accumulated only at levels distal to the lamina cribrosa (Fig. 1, F and G). This resulted in a 250% higher number of neurofilaments beyond the lamina cribrosa (e.g., 700 μm from the retinal excavation) compared with the number at levels proximal to the landmark (e.g., the 50-μm level). We refer to this phenomenon as regional neurofilament accumulation, which is defined as the percent increase in neurofilament number at the 700-μm level (or more distally) over the number at the 50-μm level (i.e., neurofilament number [700 μm − 50 μm/50 μm] × 100).

Attainment of Mature Neurofilament Subunit Stoichiometry and Interneurofilament Spacing Precede Regional Neurofilament Accumulation and Caliber Expansion

To investigate how subunit stoichiometry contributes to regional neurofilament accumulation, the subunit composition of neurofilaments from optic nerves isolated at stages throughout postnatal development was quantitated by densitometric analysis of Western blots. For comparison, we analyzed isolated neurofilaments from the intraretinal portions of optic axons where neurofilaments undergo minimal reorganization (Sanchez et al., 1996). Although the retina is composed of different cell types, the axons and perikarya of retinal ganglion cells (RGCs) contained nearly all of the NFH immunoreactivity as shown by confocal microscopic analysis of whole mount preparations of retina immunostained with anti-NFH antibodies (data not shown). Analysis of the Triton-soluble NFH pool that has been proposed to incorporate into assembled neurofilaments during development (Shea, 1994) revealed very little if any Triton-soluble NFH in the optic nerve after P10, although a pool of Triton-soluble NFH protein persisted in the retina throughout development (Fig. 2 A). NFH levels increased nearly threefold between P9 and P16 along optic axons, including intraretinal portions (Fig. 2 B). Consistent with these results, the ratio of NFH to NFL rose sharply from P6 and peaked by P12 along axons
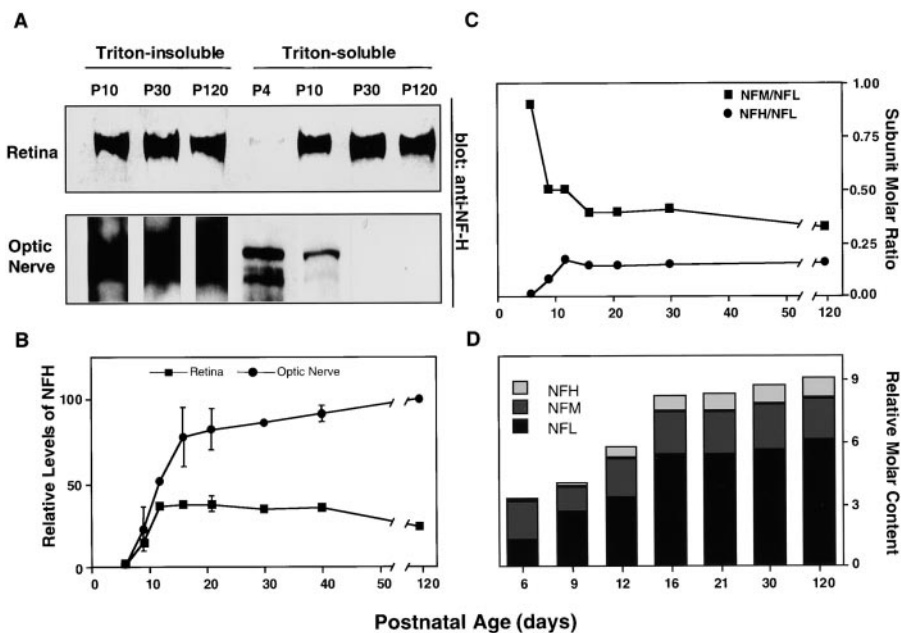
Figure 2. Regional differences in NFH protein and neurofilament subunit stoichiometry during postnatal development. (A) Western blot analysis of Triton-soluble fractions of the retina and optic nerve with the anti-NFH antibody, SMI33. (B) Relative levels of total NFH protein in Triton-insoluble fractions of optic nerve (●) and intraretinal optic axons (■) were quantified by densitometry after immunostaining with SMI33. Levels of NFH immunoreactivity are expressed relative to that in the adult optic nerve given a value of 100%. Error bars indicate SEM ($n = 4$ at each age). (C and D) The ratios of neurofilament subunits in Triton-insoluble cytoskeletons of the optic nerve during postnatal development, determined by quantitative Western blot analysis (see Materials and Methods). (C) Molar ratios of NFH to NFL and NFM to NFL at different postnatal ages. (D) The relative subunit molar ratio at different postnatal ages expressed relative to the values at P120. Relative levels of NFH, NFM, and NFL immunoreactivity were calculated from optic nerves at P120 and adjusted to the neurofilament subunit molar ratio determined after metabolic radiolabeling of optic axon proteins in vivo (NFH/NFM/NFL = 1:2:6) as described previously (Nixon and Lewis, 1986).

(Fig. 2 C), nearly 2 wk before neurofilaments began to accumulate regionally (Fig. 1 G) and well before mature axonal diameters were achieved (Fig. 1 E) (Sanchez et al., 1996). The proportions of NFM in optic axon neurofilaments decreased (Fig. 2 C) as the ratio of NFH to NFL increased. Comparing the subunit stoichiometries at different postnatal ages confirms a net reduction in NFM content on neurofilaments when NFH appears (Fig. 2 D).

In addition, changes in the distance between neurofilaments have also been suggested as a mechanism regulating neurofilament accumulation and axon caliber (de Waegh et al., 1992; Hsieh et al., 1994; Nixon et al., 1994). To investigate the timing of this event during development, we used computer-assisted morphometry to determine the distances between each neurofilament and its nearest neighbor in a representative subpopulation of optic axons from the total population at each of six postnatal ages. A significant shift in the distribution of nearest neighbor distances indicating greater interneurofilament spacing began after P9 and plateaued by P16 (Fig. 3) (P9 to P16; Kruskal and Wallis analysis, $q = 2.62$); thereafter, including time points at 21 and 30 d (not shown), average spacing did not increase ($q < 0$). The apparent difference between P16 and adult is due to a 10% reduction in the mean interneurofilament distance at 50 μm in adult axons. Comparison with regional neurofilament accumulation shows that both mature interneurofilament spacing and subunit stoichiometry are attained before the robust accumulation of neurofilaments between P21 and P30 (see Fig. 1 G).

NFH Phosphorylation during Development Occurs Sequentially: Regional Neurofilament Accumulation Coincides Selectively with RT97 Phosphoepitope Expression

To investigate the relationship of NFH COOH-terminal phosphorylation to neurofilament organization, we mea-

sured the levels of individual NFH phosphoepitopes on neurofilaments before and during the process of caliber expansion and neurofilament accumulation. To distinguish the three NFH phosphoepitopes identified by the monoclonal antibodies SMI34 and SMI31 (Sternberger and Sternberger, 1983), and RT97 (Coleman and Anderton, 1990) by biochemical means, we separated chymotryptic digests of electrophoretically purified NFH from adult optic axon neurofilaments by HPLC and analyzed individual peptide-containing fractions for SMI34, SMI31, and RT97 immunoreactivity. Some fractions containing little or no SMI31 immunoreactivity were strongly SMI34 immunoreactive (Fig. 4 A). Also, the RT97 epitope was not detected in fractions that exhibited the highest SMI31 or SMI34 immunoreactivity. To confirm these results, we immunoadsorbed equal aliquots of a tryptic digest of NFH onto either RT97 or SMI31 affinity columns (Fig. 4 B). Slot blot analyses of eluted fractions from the RT97 affinity column revealed that some fractions containing RT97 immunoreactive peptides were not detected by SMI31. By comparison, some of the fractions eluted from the SMI31 affinity column were immunoreactive to SMI31 but not to RT97, indicating that SMI31 does not recognize the RT97 epitope and that the two antibodies recognize phosphoepitopes located on distinct peptide sequences. In addition, immunoblots of the total NFH subunit pool separated by two-dimensional electrophoresis were probed with SMI33, a monoclonal antibody recognizing NFH independently of its phosphorylation state. These blots show that the adult optic nerve contains multiple isoforms of NFH, spanning a pH range of 7.1 to 5.1 (Fig. 4 C). SMI31 and SMI34 recognized NFH isoforms over a wide pH range (pH 6.8 to 5.1; not shown); however, RT97 cross-reacted only with the most acidic of these isoforms (pH 5.9 to 5.1), in agreement with previous findings suggesting that RT97 recognizes an epitope that is present only in highly phosphorylated NFH peptides (Coleman and Anderton, 1990).
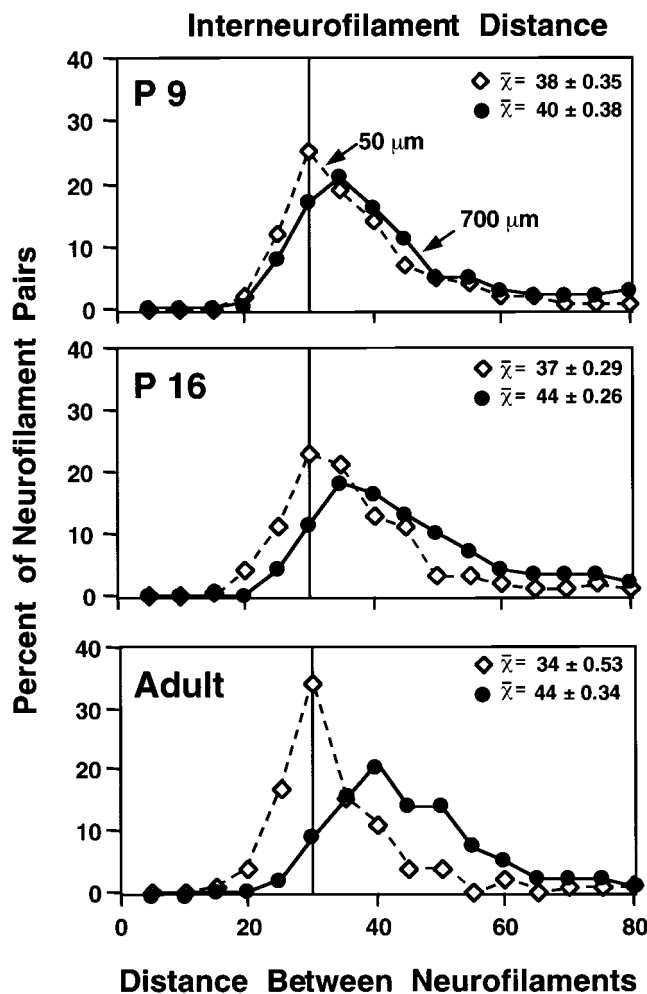
Interneurofilament Distance

P 9
◇ $\bar{x} = 38 \pm 0.35$
● $\bar{x} = 40 \pm 0.38$

50 μm

700 μm

P 16
◇ $\bar{x} = 37 \pm 0.29$
● $\bar{x} = 44 \pm 0.26$

Adult
◇ $\bar{x} = 34 \pm 0.53$
● $\bar{x} = 44 \pm 0.34$

Percent of Neurofilament Pairs

Distance Between Neurofilaments

Figure 3. Region-specific shifts in interneurofilament spacing during postnatal development. At each postnatal age, the nearest neighbor distance was calculated for every neurofilament in axons of calibers representative of those in the total axonal population at the 50-μm (◇) and 700-μm (●) levels of the optic nerve (see Materials and Methods). Mean interfilament distances (SEM) are given for 1,175–2,500 neurofilaments at each axon level and postnatal age. Significant regional differences in interneurofilament spacing were detected as early as P9 ($q = 2.06$; Kruskal and Wallis analysis). A gradual shift to larger interneurofilament spacing was observed only at 700 μm between P9 and P16; thereafter, spacing remained unchanged ($q = 2.62$ and $q < 0$, respectively; Kruskal and Wallis analysis).

Next, we compared the levels of individual NFH phosphoepitopes within Triton-insoluble neurofilament fractions from either the optic nerves, which contain principally the expanding portions of RGC axons, or the retinas, which contain unexpanded portions of the same axons. The assay was first standardized to determine saturation levels by using quantitative densitometry of adult optic nerve NFH protein immunoblots. The extent of NFH COOH-terminal phosphorylation greatly exceeded the increase in total NFH levels during development (Fig. 5). RT97, SMI31, and SMI34 immunoreactivity exhibited distinctive temporal and regional patterns (Fig. 5, A and B). Levels of SMI34 immunoreactivity reached near maximal levels by P9 equally in both intraretinal and extraretinal

portions of optic axons (Fig. 5, A and B). In contrast to SMI34, the SMI31 and RT97 phosphoepitopes rose to higher levels on neurofilaments from optic axons than those from intraretinal portions of the same axons, suggesting that these epitopes play a selective role in expanding axons. Regional differences in SMI31 levels were detected as early as P9 and were maximal by P16 (Fig. 5 D). By contrast, the RT97 phosphoepitope remained at negligible levels in the retina and was first detected in optic axons only after the third postnatal week (Fig. 5 B), increasing linearly in amount until P120. Its late appearance was not due to lower expression levels of NFH during early development because equal amounts of NFH protein from P30 and P120 optic nerves yielded the expected 2.5-fold increase in RT97 immunoreactivity (Fig. 5 C). The appearance and rise of RT97 immunoreactivity between P21 and P120 coincided with the onset and rise of regional neurofilament accumulation (compare Figs. 1 G and 5 B).

Preservation of Regional Neurofilament Accumulation in NFH-deleted Mice Is Accompanied by Selectively Increased Generation of the RT97 Phosphoepitope on NFM

Because the small phenotypic effects of NFH gene ablation in peripheral motor neurons (Elder et al., 1998b; Rao et al., 1998; Zhu et al., 1998) have raised questions about the importance of NFH to neurofilament number specification, we investigated whether or not NFM assumes important aspects of NFH function in NFH-deleted mice. The cross-sectional areas of optic axons in NFH-null mice were reduced 12% (0.302 ± 0.013 vs. 0.265 ± 0.020 μm², $P < 0.01$) or 16% (0.560 ± 0.035 vs. 0.438 ± 0.024 μm², $P < 0.01$) at the 50- and 700-μm levels, respectively, reflecting mainly a reduced proportion of the largest caliber axons (Fig. 6 A), as previously seen for motor axons (Elder et al., 1998b; Rao et al., 1998). NFH gene deletion had relatively small effects on regional axonal expansion (Fig. 6 B) or regional accumulation of neurofilaments as defined in this study ($P = 0.05$) (Fig. 6 B). NFM levels were not elevated in optic nerves of NFH-deleted mice (Fig. 6 C) in contrast to motor neurons (data not shown) (Rao et al., 1998). Similarly, the levels of SMI31 immunoreactivity on this subunit were unchanged and no generation of the SMI34 epitope was evident on NFM (Fig. 6 C). By contrast, RT97 immunoreactivity on NFM was substantially increased in NFH-deleted mice (Fig. 6 D). Because RT97 detects a series of NFH breakdown products that extend below the molecular mass range of NFM (Fig. 6 D), one-dimensional gels were inadequate to discriminate accurately the contributions of RT97 on NFH and NFM in the optic axons of wild-type mice. This increase was more clearly seen in peripheral nerves where NFH breakdown products were less prominent (inset, Fig. 6 E). Two-dimensional polyacrylamide gel analyses (Fig. 6 E) of optic nerve did partially separate NFM from NFH breakdown products and showed that RT97 immunoreactivity associated with NFM was elevated in NFH-null mice. Little apparent RT97 labeling of NFM was evident in NFH^{+/+} mice when NFH breakdown products were largely separated by isoelectric focusing from the region of the gel containing NFM. The position of NFM relative to NFH was confirmed by reprobing the blot in Fig. 6, D and E,
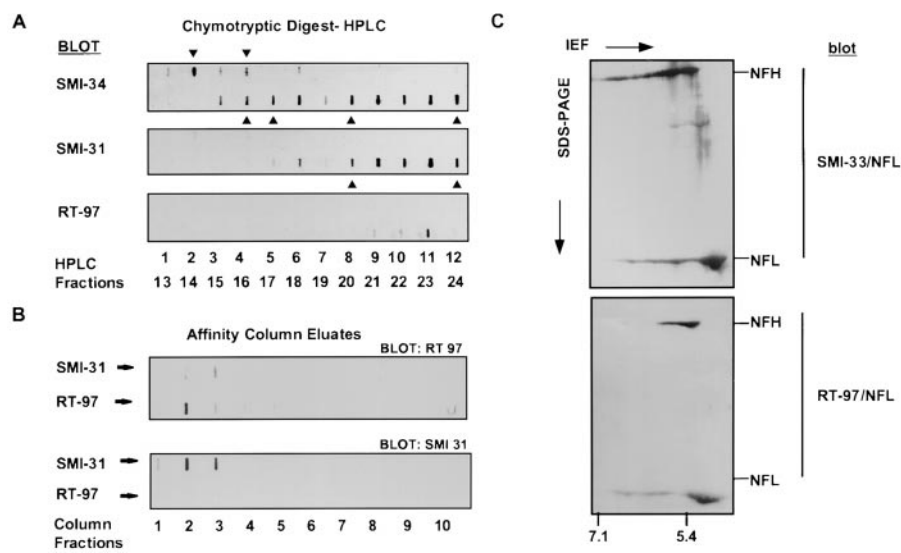
Figure 4. SMI31 and RT97 are distinct NFH phosphoepitopes. (A) NFH peptides after chymotryptic digestion were separated by HPLC, and aliquots of all fractions were immunostained in slot blots with SMI34, SMI31, or RT97. Fractions containing high SMI34 or SMI31 signal and no RT97 signal are indicated by arrowheads. (B) NFH tryptic digest peptides after tryptic digestion were affinity purified with either RT97 or SMI31 antibodies. The slot blots of eluted fractions from SMI31 and RT97 affinity columns probed with RT97 antibody (top panel) or with SMI31 antibody (bottom panel). (C) Two-dimensional PAGE immunoblots of NFH from adult optic nerve cytoskeletal fractions probed with SMI33 to detect total NFH or the RT97 phosphoepitope. All blots were also immunostained with an antibody against NFL used as an internal standard to confirm the pH range. RT97 recognizes only the most acidic (highly phosphorylated) NFH isoforms (pH 5.9 to 5.1). IEF, Isoelectric focusing.

with RM04. The RT97 immunoreactive signal associated with NFM was estimated to be 5–10% of the signal associated with NFH, based on multiple two-dimensional immunoblots of optic axons developed for equivalent times or on one-dimensional blots of peripheral nerve. Other evidence implies that a relatively small proportion of the total RT97 immunoreactivity on NFH or on NFM in NFH-null mice may be sufficient to establish normal regional neurofilament accumulation. Neurofilament accumulation at 700 μm had plateaued by P30 (see Fig. 1 F), even though RT97 levels were only one third of the level at P120 (see Fig. 5 B). Moreover, RT97 levels increase even further with age (data not shown), indicating that the level of RT97 associated with the phase of rapid neurofilament accumulation may be a very small fraction of the RT97 level on NFH in the mature adult. A similar effect on NFM phosphorylation was seen in the spinal cord (data not shown) where we also confirmed a previously observed modest increase (less than twofold) in NFM levels (Rao et al., 1998). Thus, when NFH is deleted, at least one of its characteristic properties, the RT97 phosphoepitope, is partially assumed by NFM.
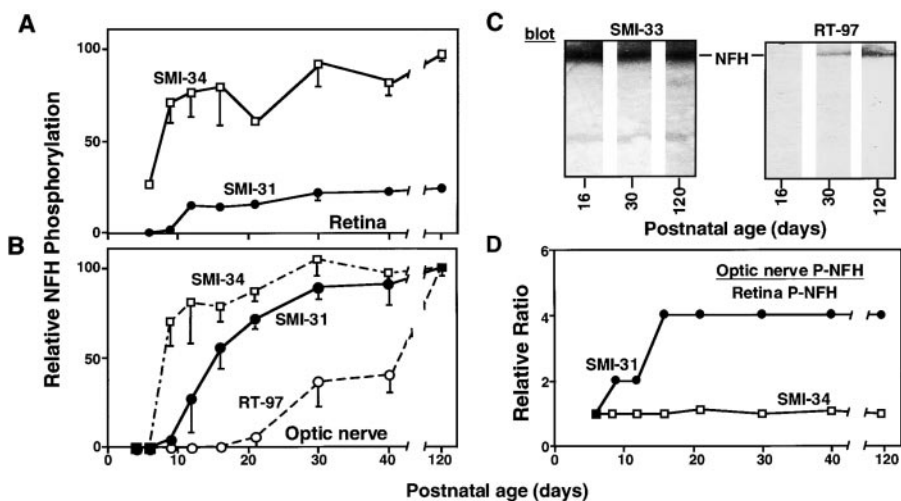

Figure 5. Sequential appearance of distinct phosphoepitopes on NFH during development. (A) Relative content of different phosphoepitopes associated with NFH in Triton-insoluble cytoskeletal fractions from intraretinal axons (A) and optic nerves (B) from mice at varying postnatal ages. Each data point represents the immunoreactivity level of a given phosphoepitope expressed as the ratio to total NFH immunoreactivity determined with SMI33 antibody. No RT97 immunoreactivity was detected in retinal axons. Each point is the mean and standard error of separate determinations from four different sets of pooled retinas or optic nerve segments (see Materials and Methods). (C) Immunoblots of neurofilament fractions from optic nerves from P16, P30, and P120 mice containing equal amounts of NFH protein probed with SMI33 (left) and a duplicate blot probed with RT97 antibodies (right). (D) The establishment of regional differences along axons in the content of individual NFH phosphoepitopes during postnatal development. To emphasize regional differences, the content of SMI31 or SMI34 in neurofilaments is expressed as a ratio of the optic nerve (optic axons) to retina (intraretinal RGC axons) values. Values >1 reflect a relative increase in content in the optic nerves. RT97 is not included in D because it was not detectable in intraretinal axons.
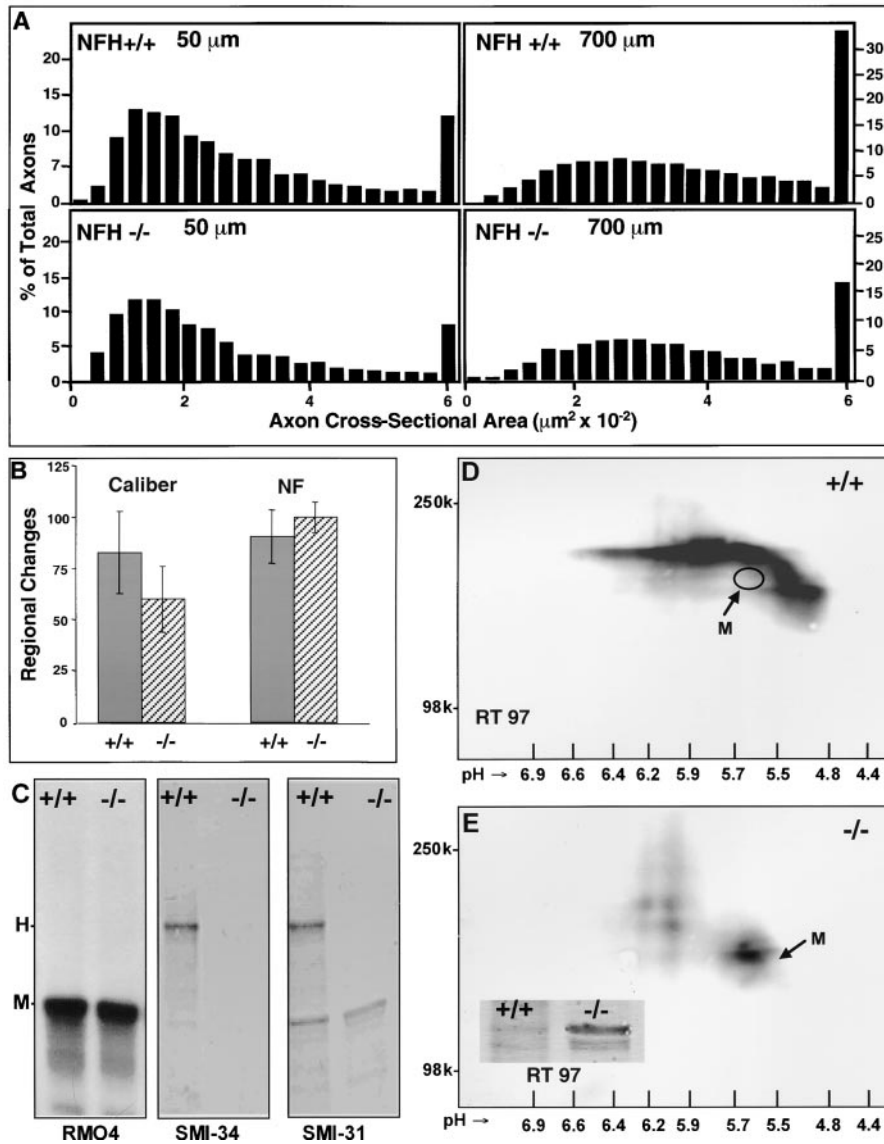
Figure 6. Axonal morphometry and neurofilament subunit phosphorylation in optic axons of NFH-null mice. (A) Axon caliber distributions at optic nerve levels 50 and 700 μm from the eye in NFH$^{+/+}$ and NFH$^{-/-}$ mice. The number of axons in each size class, expressed as a percentage of the total axonal population analyzed, is plotted as a function of axon cross-section area. A total of 9,864 axons from 5 wild-type and 5 NFH-null optic nerves were analyzed at each axonal level. (B) Regional axonal expansion (mean caliber [700 μm − 50 μm/50 μm] × 100) for the populations of axons in A. Mean regional neurofilament accumulation (neurofilament number [700 μm − 50 μm/50 μm] × 100) for 1,350 axons of caliber size representative of the whole fiber population. Lower regional differences in these 1.5-yr-old mice compared with 4-mo-old mice in Fig. 1 are due to aging-related increases in caliber and neurofilament number at the 50-μm level (Nixon, R.A., unpublished data). (C–E) Neurofilament subunit levels and phosphorylation in control and NFH-null mice. (C) Total NFM levels are not altered when detected with a phosphorylation-independent neurofilament antibody to NFM (RM04) generously provided by Dr. Virginia Lee (University of Pennsylvania, Philadelphia, PA. Representative examples of one-dimensional electroblots ($n = 4$) immunostained with SMI34 and SMI31 show no compensatory increase in levels of these phosphoepitopes in NFH$^{-/-}$ mice. Two-dimensional immunoblots of optic nerves from NFH$^{+/+}$ (D) and NFH$^{-/-}$ (E) mice stained with RT97 demonstrate the absence of NFH and presence of RT97-positive NFM in NFH$^{-/-}$ mice. The identity and precise position of NFM in D (indicated by oval) were confirmed by reprobing the blots with RM04 (data not shown). The smaller quantity of NFH breakdown products in sciatic nerve samples allowed increases of RT97 on NFM in null mice to be appreciated (E, inset).

Selectively Reduced RT97 Phosphoepitope Levels Are Associated with Decreased Regional Neurofilament Accumulation in Myelin-deficient Shiverer Mutant Mice

Mutations in the MBP gene in Shiverer mice (*shi/shi*) inhibit oligodendroglial investment of most axons and prevent them from receiving signals that trigger regional accumulation of neurofilaments (Sanchez et al., 1996), although neurofilaments in these axons achieve normal interneurofilament spacing (Fig. 7 A). The percentage of axons that do become invested by oligodendroglial cells equals the extent of regional neurofilament accumulation observed (~35% of normal accumulation) (Sanchez et al., 1996) (Fig. 7 B). Thus, the Shiverer mice provided a suitable model to establish whether or not RT97 phosphoepitope expression may be selectively involved in the glial signaling process that regulates regional neurofilament accumulation. Relative levels of the SMI34, SMI31, and RT97 phosphoepitopes were quantitated in NFH subunits of axonal neurofilament fractions from optic nerves of Shiverer mice lacking the MBP gene (*shi/shi*) (Shine et al., 1992) and mice expressing the normal level of MBP protein (Fig. 7 C). Neurofilaments from *shi/shi* optic axons contained 32% of the RT97 immunoreactivity detected in heterozygous or wild-type mice. This reduction in RT97 phosphoepitope levels was equivalent to the proportion of axons that fail to achieve regional neurofilament accumulation. By contrast, SMI31 and SMI34 phosphoepitope levels in NFH subunits from *shi/shi* mice were normal (Fig. 7 C). Immunoelectron microscopy indicated that RT97 immunoreactivity was not uniformly reduced in Shiverer axons. Axons invested by oligodendroglial cells or primitive myelin sheaths exhibited near normal levels of RT97 immunoreactivity (Fig. 7 D),
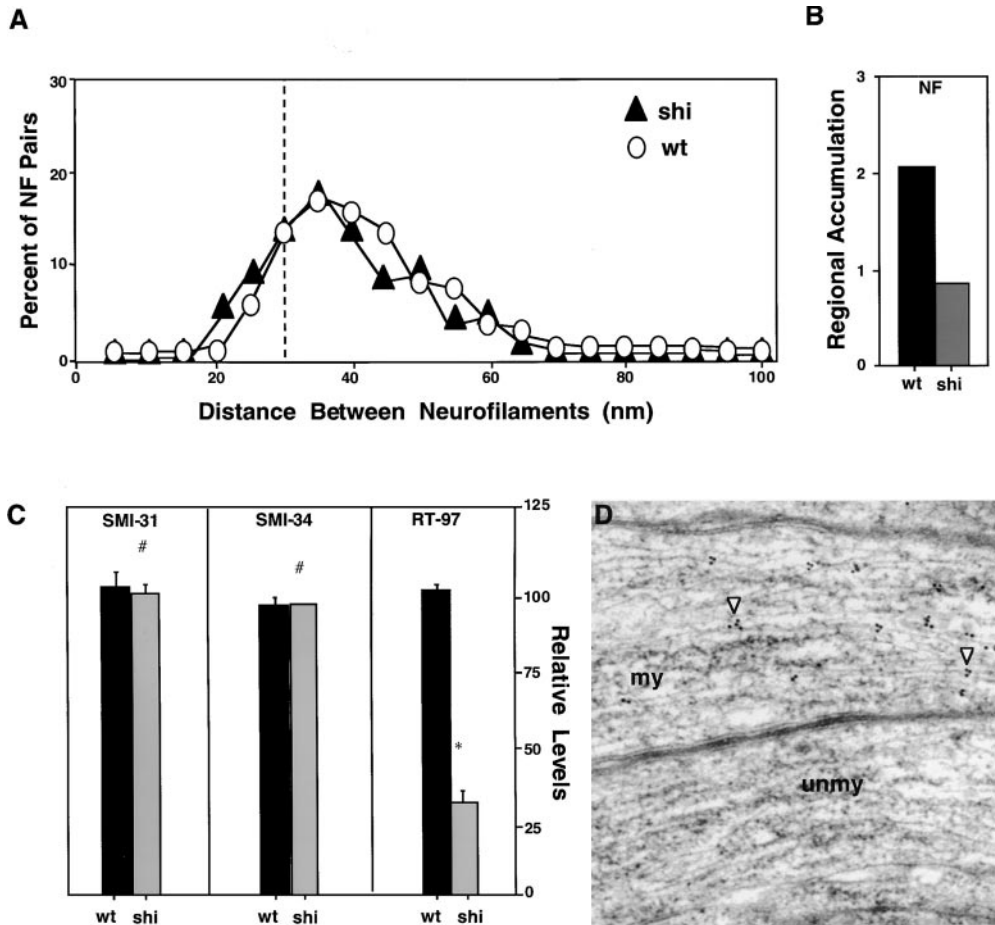
Figure 7. Regional neurofilament accumulation and RT97 epitope levels are selectively and markedly reduced in Shiverer mutant mice. (A) Interneurofilament spacing in optic axons (700-μm level) of 3-month-old Shiverer mice (▲, shi) is similar to that of wild-type mice (○, wt). (B) Regional neurofilament accumulation (neurofilament number [700 μm − 50 μm/50 μm] × 100) was determined in >300 optic axons at the 50- and 700-μm levels for three wild-type or Shiverer homozygous mice. (C) SMI34, SMI31, and RT97 immunoreactivities as a ratio of total NFH (SMI33) immunoreactivity were determined in the same groups of mice by quantitative densitometry. All values are expressed relative to the wild-type control set at 100%. Each value represents the mean and standard error from four separate samples (*$P < 0.05$ and #$P > 0.05$ by Student's t test). Immuno-electron microscopy of the RT97 epitope in axons of normal and homozygous Shiverer mice. After incubation of treated epon sections with RT97 (see Materials and Methods), 5-nm gold-conjugated secondary antibody decorated neurofilaments in normal optic axons (not shown) and (D) Shiverer axons associated with primitive myelin sheaths (my; arrowhead). No RT97 immunoreactivity was detected in unmyelinated axons (unmy) from Shiverer mice.

whereas the ~65% of axons lacking myelin or glial investment were completely unlabeled.

Discussion

Changes in NFH expression, neurofilament subunit stoichiometry, or interneurofilament spacing have previously been proposed to contribute to the regional accumulation of neurofilaments and expansion of myelinated axons (Lee et al., 1993; Nixon, 1998a); however, we establish here that such changes in neurofilament properties largely precede these growth processes. Like neurofilament number, interneurofilament spacing was also modulated regionally although its relationship to myelination and radial growth is complex. Interneurofilament spacing increases along portions of optic axons invested with oligodendrocytes, but a similar change also occurs along distal portions of unmyelinated axons, which do not expand (Nixon et al., 1994; Sanchez et al., 1996). The absence of a clear relationship between interneurofilament spacing and radial growth is also evident in neurofilament transgenic and gene-targeted mice, which exhibit normal filament spacing despite varying changes in caliber (Marszalek et al., 1996; Xu et al., 1996; Elder et al., 1998a,b; Rao et al., 1998; Zhu et al., 1998).

Role of Subunit Stoichiometry during Regional Neurofilament Accumulation and Caliber Expansion

We found that as the proportions of NFH in neurofilaments increased during early postnatal development NFM subunit content of neurofilaments decreased commensurately, suggesting that NFH may compete with NFM in binding to NFL or forming 10-nm filaments as proposed previously by Marszalek et al. (1996). These striking changes in neurofilament composition, however, were complete nearly 2 wk before axon calibers expanded regionally. Targeted disruption of the NFH gene diminishes the radial growth of large motor axons to varying degrees (Elder et al., 1998b; Rao et al., 1998; Zhu et al., 1998), although these effects are unexpectedly small given the role suspected for NFH in radial growth. We found comparably small effects on optic axon calibers and showed that regional neurofilament accumulation was also minimally affected. However, the ability of other proteins to assume the functions of a deleted protein is not uncommon in gene ablation studies. In the case of NFH deletion, caliber re-

ductions appear to have been offset by several compensatory mechanisms in different fiber systems. Microtubules were substantially increased (Rao et al., 1998; Zhu et al., 1998) and, in one mouse model where microtubule increases could not be demonstrated, caliber reductions were greater (Elder et al., 1998b). The loss of NFH was also accompanied by elevated NFM levels (Rao et al., 1998; Zhu et al., 1998) and possibly by greater NFM phosphorylation (Zhu et al., 1998), although, in two studies, phosphate addition to known sites on NFM (e.g., SMI31) was not increased (Elder et al., 1998b; Rao et al., 1998). The NFM compensatory response is significant in light of evidence that NFM is required to achieve normal axon caliber (Elder et al., 1998a). What is now clear from our studies of optic axons from NFH-deleted mice is that preservation of the capacity to accumulate neurofilaments regionally is accompanied by the selective appearance of the RT97 phosphoepitope on NFM, which is normally an NFH-specific phosphorylation event. Moreover, the normal 2:1 stoichiometry of NFM to NFH (Nixon and Lewis, 1986) and the increase in NFM in some fiber tracts (Rao et al., 1998; our findings) results in a greater capacity of NFM to rescue NFH function in NFH-deleted mice. Even though levels of RT97 signal on NFM are lower than those on NFH, our evidence indicates that only a small proportion of the total RT97 epitope level is normally present during the period of robust neurofilament accumulation. Levels of RT97 are undetectable in Shiverer axons that are not invested with an oligodendroglial cell, whereas the smaller population of axons with primitive myelin sheaths had normal or near normal levels of RT97. These findings, therefore, suggest that axons are able to compensate partially for NFH's functions and highlight a particularly critical role of NFM and phosphorylation generating the RT97 epitope.

Delayed Appearance of the RT97 Phosphoepitope on NFH Is Selectively Associated with Regional Neurofilament Accumulation

Two distinct NFH phosphorylation events preceded appearance of the RT97 phosphoepitope and were shown to be regulated independently of both RT97-related phosphorylation and regional neurofilament accumulation. The appearance of the SMI34 phosphoepitope coincided with the first detection of NFH protein and reflected phosphorylation of KSPXX motifs along its COOH terminus (Pant and Veeranna, 1995). We observed that NFH subunits initially appearing in the optic nerve had nearly peak levels of this phosphoepitope (i.e., nearly maximal SMI34/SMI33 ratios), indicating that phosphorylation at this site is essentially complete by the time transported neurofilaments reach the level of the optic nerve. This conclusion is consistent with immunocytochemical evidence that SMI34 and Erk1/2, the kinase(s) believed to generate the SMI34 epitope on NFH (Roder and Ingram, 1991; Pant and Veeranna, 1995; Veeranna et al., 1998), are enriched in ganglion cell perikarya (Sanchez, I., L. Hassinger, T. Wheelock, G. Hauser, and R.A. Nixon. 1996. *Soc. Neurosci.* 22: 775.7 [Abstr.]). The appearance of SMI34 on NFH subunits still within ganglion cell perikarya suggests a role for this phosphorylation event early after NFH synthesis.

The subsequent appearance of the SMI31 epitope also preceded regional neurofilament accumulation. Our findings support the hypothesis that SMI31 generation may be related to changes in interneurofilament spacing, in agreement with earlier findings that both interneurofilament spacing and SMI31 immunoreactivity are lower at nodes of Ranvier than along internodal regions (Mata et al., 1992). Both SMI31 immunoreactivity and interneurofilament spacing were normal in Shiverer mutant mice, even though RT97 levels and regional neurofilament accumulation were markedly reduced (see Fig. 7). These observations establish that neither interneurofilament spacing nor phosphorylation represented by the SMI31 epitope regulates regional caliber expansion.

The delayed appearance of RT97 during postnatal development is the only change in neurofilament properties that coincides with the late onset of regional axon caliber expansion during development, parallels the rate of recruitment of axons for radial growth, and segregates selectively within regions of the axon that undergo neurofilament accumulation. Moreover, among the various properties of neurofilaments that change during development, only RT97 levels and regional accumulation are affected when glia-to-axon signaling is blocked in Shiverer mutant mice. When the NFH gene is deleted in mice, the RT97 epitope increases specifically on NFM, allowing this subunit to substitute partially the phosphorylation function of NFH. This result implies that additional tests of the role of KSP phosphorylation on neurofilament function using an in vivo genetic approach will require replacing both NFH and NFM with the appropriate subunits mutagenized at the appropriate sites.

The foregoing results strongly support the conclusion that phosphorylation of a subset of KSP sites is a key aspect of the regulation of neurofilament number in axons during axonal radial growth. RT97 appearance can be viewed as the culmination of a series of developmental events such as NFH expression and proper neurofilament subunit composition and SMI34/SMI31 phosphorylation, which may serve as critical antecedents to the process of neurofilament accumulation and radial growth under normal conditions. Two hypothetical functions of RT97 generation that remain to be tested are its role as an actual trigger of neurofilament accumulation or, alternatively, as a critical neurofilament modification required to stabilize the neurofilament/cytoskeletal after neurofilaments accumulate. Supporting the former possibility are observations that NFH and NFM phosphorylation slows neurofilament transport (Lewis and Nixon, 1988; Archer et al., 1994). Moreover, neurofilaments containing the most highly phosphorylated isoforms of NFH, shown in this study to have the RT97 phosphoepitope, have the slowest net movement (Yabe et al., 2000) and are retained along axons for long periods (Lewis and Nixon, 1988), presumably associated with a nonuniform stationary, but dynamically turning over axonal cytoskeletal network (Hirokawa et al., 1984; Nixon and Logvinenko, 1986; Nixon, 1998a). As proposed previously (Sanchez et al., 1996), abrupt shifts in the number of neurofilaments within a given region of the axon could be induced by local changes in a particular protein kinase or phosphatase activity that modulates the strength of interactions between neurofilaments and the axonal transport machinery, stationary axonal elements, or both. Phosphorylation may also promote stability of these neurofilaments by reducing their susceptibility to

proteases (Goldstein et al., 1987; Pant, 1988). The presence of the RT97 phosphoepitope on tau (Brion et al., 1993) and microtubule-associated protein 1B (Johnstone et al., 1997) during early development suggests that other potentially interacting cytoskeletal elements regulated by RT97-generating protein kinase(s) may also contribute to regional maturation of the axonal cytoskeleton. Characterizing the intercellular and intraneuronal mechanisms regulating this phosphorylation event should help to reveal how different patterns of pathologic neurofilament accumulation arise in human neurodegenerative diseases.

References

Archer, D.R., D.F. Watson, and J.W. Griffin. 1994. Phosphorylation-dependent immunoreactivity of neurofilaments and the rate of slow axonal transport in the central and peripheral axons of the rat dorsal root ganglion. *J. Neurochem.* 62:1119–1125.

Bajaj, N.P., and C.C. Miller. 1997. Phosphorylation of neurofilament heavy-chain side-arm fragments by cyclin-dependent kinase-5 and glycogen synthase kinase-3alpha in transfected cells. *J. Neurochem.* 69:737–743.

Bennett, G.S., U. Basu, B.A. Hollander, R. Quintana, and R. Rodriguez. 1994. Differential sensitivity to inhibitors discriminates between two types of kinases responsible for in vivo phosphorylation of the carboxy-terminal tail of chicken neurofilament-M. *Mol. Cell. Neurosci.* 5:358–368.

Brion, J.P., A.M. Couck, J. Robertson, T.L. Loviny, and B.H. Anderton. 1993. Neurofilament monoclonal antibodies RT97 and 8D8 recognize different modified epitopes in paired helical filament-tau in Alzheimer's disease. *J. Neurochem.* 60:1372–1382.

Carden, M.J., J.Q. Trojanowski, W.W. Schlaepfer, and V.M. Lee. 1987. Two-stage expression of neurofilament polypeptides during rat neurogenesis with early establishment of adult phosphorylation patterns. *J. Neurosci.* 7:3489–3504.

Chernoff, G.F. 1981. Shiverer: an autosomal recessive mutant mouse with myelin deficiency. *J. Hered.* 72:128.

Ching, G.Y., and R.K. Liem. 1993. Assembly of type IV neuronal intermediate filaments in nonneuronal cells in the absence of preexisting cytoplasmic intermediate filaments. *J. Cell Biol.* 122:1323–1335.

Chiu, F.C., and W.T. Norton. 1982. Bulk preparation of CNS cytoskeleton and the separation of individual neurofilament proteins by gel filtration: dye-binding characteristics and amino acid compositions. *J. Neurochem.* 39:1252–1260.

Clark, E.A., and V.M. Lee. 1991. Dynamics of mammalian high-molecular-weight neurofilament subunit phosphorylation in cultured rat sympathetic neurons. *J. Neurosci. Res.* 30:116–123.

Colello, R.J., U. Pott, and M.E. Schwab. 1994. The role of oligodendrocytes and myelin on axon maturation in the developing rat retinofugal pathway. *J. Neurosci.* 14:2594–2605.

Coleman, M.P., and B.H. Anderton. 1990. Phosphate-dependent monoclonal antibodies to neurofilaments and Alzheimer neurofibrillary tangles recognize a synthetic phosphopeptide. *J. Neurochem.* 54:1548–1555.

Collard, J.F., F. Cote, and J.P. Julien. 1995. Defective axonal transport in a transgenic mouse model of amyotrophic lateral sclerosis. *Nature.* 375:61–64.

Cote, F., J.F. Collard, and J.P. Julien. 1993. Progressive neuronopathy in transgenic mice expressing the human neurofilament heavy gene: a mouse model of amyotrophic lateral sclerosis. *Cell.* 73:35–46.

de Waegh, S.M., V.M. Lee, and S.T. Brady. 1992. Local modulation of neurofilament phosphorylation, axonal caliber, and slow axonal transport by myelinating Schwann cells. *Cell.* 68:451–463.

Elder, G.A., V.L. Friedrich, Jr., P. Bosco, C. Kang, A. Gourov, P.H. Tu, V.M. Lee, and R.A. Lazzarini. 1998a. Absence of the midsized neurofilament subunit decreases axonal calibers, levels of light neurofilament (NF-L), and neurofilament content. *J. Cell Biol.* 141:727–739.

Elder, G.A., V.L. Friedrich, Jr., C. Kang, P. Bosco, A. Gourov, P.H. Tu, B. Zhang, V.M. Lee, and R.A. Lazzarini. 1998b. Requirement of heavy neurofilament subunit in the development of axons with large calibers. *J. Cell Biol.* 143:195–205.

Elhanany, E., H. Jaffe, W.T. Link, D.M. Sheeley, H. Gainer, and H.C. Pant.

1994. Identification of endogenously phosphorylated KSP sites in the high-molecular-weight rat neurofilament protein. *J. Neurochem.* 63:2324–2335.

Eyer, J., and A. Peterson. 1994. Neurofilament-deficient axons and perikaryal aggregates in viable transgenic mice expressing a neurofilament-beta-galactosidase fusion protein. *Neuron.* 12:389–405.

Goldberg, S., and B. Frank. 1979. The guidance of optic axons in the developing and adult mouse retina. *Anat. Rec.* 193:763–774.

Goldstein, M.E., N.H. Sternberger, and L.A. Sternberger. 1987. Phosphorylation protects neurofilaments against proteolysis. *J. Neuroimmunol.* 14:149–160.

Gotow, T., and J. Tanaka. 1994. Phosphorylation of neurofilament H subunit as related to arrangement of neurofilaments. *J. Neurosci. Res.* 37:691–713.

Gotow, T., T. Tanaka, Y. Nakamura, and M. Takeda. 1994. Dephosphorylation of the largest neurofilament subunit protein influences the structure of crossbridges in reassembled neurofilaments. *J. Cell Sci.* 107:1949–1957.

Graf von Keyserlingk, D., and U. Schramm. 1984. Diameter of axons and thickness of myelin sheaths of the pyramidal tract fibres in the adult human medullary pyramid. *Anat. Anz.* 157:97–111.

Guidato, S., L.H. Tsai, J. Woodgett, and C.C. Miller. 1996. Differential cellular phosphorylation of neurofilament heavy side-arms by glycogen synthase kinase-3 and cyclin-dependent kinase-5. *J. Neurochem.* 66:1698–1706.

Hirokawa, N., M.A. Glicksman, and M.B. Willard. 1984. Organization of mammalian neurofilament polypeptides within the neuronal cytoskeleton. *J. Cell Biol.* 98:1523–1536.

Hisanaga, S., S. Yasugawa, T. Yamakawa, E. Miyamoto, M. Ikebe, M. Uchiyama, and T. Kishimoto. 1993. Dephosphorylation of microtubule-binding sites at the neurofilament-H tail domain by alkaline, acid, and protein phosphatases. *J. Biochem. (Tokyo).* 113:705–709.

Hoffman, P.N., R.J. Lasek, J.W. Griffin, and D.L. Price. 1983. Slowing of the axonal transport of neurofilament proteins during development. *J. Neurosci.* 3:1694–1700.

Hsieh, S.T., G.J. Kidd, T.O. Crawford, Z. Xu, W.M. Lin, B.D. Trapp, D.W. Cleveland, and J.W. Griffin. 1994. Regional modulation of neurofilament organization by myelination in normal axons. *J. Neurosci.* 14:6392–6401.

Johnstone, M., R.G. Goold, I. Fischer, and P.R. Gordon-Weeks. 1997. The neurofilament antibody RT97 recognises a developmentally regulated phosphorylation epitope on microtubule-associated protein 1B. *J. Anat.* 191:229–244.

Laemmli, U.K. 1970. Cleavage of structural proteins during the assembly of the head of bacteriophage T4. *Nature.* 227:680–685.

Lee, M.K., Z. Xu, P.C. Wong, and D.W. Cleveland. 1993. Neurofilaments are obligate heteropolymers in vivo. *J. Cell Biol.* 122:1337–1350.

Leterrier, J.F., J. Kas, J. Hartwig, R. Vegners, and P.A. Janmey. 1996. Mechanical effects of neurofilament cross-bridges. Modulation by phosphorylation, lipids, and interactions with F-actin. *J. Biol. Chem.* 271:15687–15694.

Lewis, S.E., and R.A. Nixon. 1988. Multiple phosphorylated variants of the high molecular mass subunit of neurofilaments in axons of retinal cell neurons: characterization and evidence for their differential association with stationary and moving neurofilaments. *J. Cell Biol.* 107:2689–2701.

Marszalek, J.R., T.L. Williamson, M.K. Lee, Z. Xu, P.N. Hoffman, M.W. Becher, T.O. Crawford, and D.W. Cleveland. 1996. Neurofilament subunit NF-H modulates axonal diameter by selectively slowing neurofilament transport. *J. Cell Biol.* 135:711–724.

Mata, M., N. Kupina, and D.J. Fink. 1992. Phosphorylation-dependent neurofilament epitopes are reduced at the node of Ranvier. *J. Neurocytol.* 21:199–210.

Nixon, R.A. 1998a. Dynamic behavior and organization of cytoskeletal proteins in neurons: reconciling old and new findings. *Bioessays.* 20:798–807.

Nixon, R.A. 1998b. The slow axonal transport of cytoskeletal proteins. *Curr. Opin. Cell Biol.* 10:87–92.

Nixon, R.A., and S.E. Lewis. 1986. Differential turnover of phosphate groups on neurofilament subunits in mammalian neurons in vivo. *J. Biol. Chem.* 261:16298–16301.

Nixon, R.A., and K.B. Logvinenko. 1986. Multiple fates of newly synthesized neurofilament proteins: evidence for a stationary neurofilament network distributed nonuniformly along axons of retinal ganglion cell neurons. *J. Cell Biol.* 102:647–659.

Nixon, R.A., P.A. Paskevich, R.K. Sihag, and C.Y. Thayer. 1994. Phosphorylation on COOH terminus domains of neurofilament proteins in retinal ganglion cell neurons in vivo: influences on regional neurofilament accumulation, interneurofilament spacing, and axon caliber. *J. Cell Biol.* 126:1031–1046.

O'Farrell, P.H. 1975. High resolution two-dimensional electrophoresis of proteins. *J. Biol. Chem.* 250:4007–4021.

Ohara, O., Y. Gahara, T. Miyake, H. Teraoka, and T. Kitamura. 1993. Neurofilament deficiency in quail caused by nonsense mutation in neurofilament-L gene. *J. Cell Biol.* 121:387–395.

Pant, H. 1988. Dephosphorylation of neurofilament protein enhances their susceptibility to degeneration by calpain. *Biochemistry.* 2556:665–688.

Pant, H.C., and Veeranna. 1995. Neurofilament phosphorylation. *Biochem. Cell Biol.* 73:575–592.

Rao, M.V., M.K. Houseweart, T.L. Williamson, T.O. Crawford, J. Folmer, and D.W. Cleveland. 1998. Neurofilament-dependent radial growth of motor axons and axonal organization of neurofilaments does not require the neurofilament heavy subunit (NF-H) or its phosphorylation. *J. Cell Biol.* 143:171–181.

Roder, H.M., and V.M. Ingram. 1991. Two novel kinases phosphorylate tau and the KSP site of heavy neurofilament subunits in high stoichiometric ratios. *J. Neurosci.* 11:3325–3343.

Sanchez, I., L. Hassinger, P.A. Paskevich, H.D. Shine, and R.A. Nixon. 1996. Oligodendroglia regulate the regional expansion of axon caliber and local

accumulation of neurofilaments during development independently of myelin formation. *J. Neurosci*. 16:5095–5105.

Shea, T.B. 1994. Triton-soluble phosphovariants of the high molecular weight neurofilament subunit from NB2a/d1 cells are assembly-competent. Implications for normal and abnormal neurofilament assembly. *FEBS Lett*. 343:131–136.

Shetty, K.T., W.T. Link, and H.C. Pant. 1993. cdc2-like kinase from rat spinal cord specifically phosphorylates KSPXK motifs in neurofilament proteins: isolation and characterization. *Proc. Natl. Acad. Sci. USA*. 90:6844–6848.

Shine, H.D., C. Readhead, B. Popko, L. Hood, and R.L. Sidman. 1992. Morphometric analysis of normal, mutant, and transgenic CNS: correlation of myelin basic protein expression to myelinogenesis. *J. Neurochem*. 58:342–349.

Sihag, R.K., and R.A. Nixon. 1989. In vivo phosphorylation of distinct domains of the 70-kilodalton neurofilament subunit involves different protein kinases [published erratum at 264:4264]. *J. Biol. Chem*. 264:457–464.

Sternberger, L.A., and N.H. Sternberger. 1983. Monoclonal antibodies distinguish phosphorylated and nonphosphorylated forms of neurofilaments in situ. *Proc. Natl. Acad. Sci. USA*. 80:6126–6130.

Sun, D., C.L. Leung, and R.K.H. Liem. 1996. Phosphorylation of the high molecular weight neurofilament protein (NF-H) by Cdk5 and p35. *J. Biol. Chem*. 271:14245–14251.

Towbin, H., T. Staehelin, and J. Gordon. 1979. Electrophoretic transfer of proteins from polyacrylamide gels to nitrocellulose sheets: procedure and some applications. *Proc. Natl. Acad. Sci. USA*. 76:4350–4354.

Veeranna, N.D. Amin, N.G. Ahn, H. Jaffe, C.A. Winters, P. Grant, and H.C. Pant. 1998. Mitogen-activated protein kinases (Erk1,2) phosphorylate Lys-Ser-Pro (KSP) repeats in neurofilament proteins NF-H and NF-M. *J. Neurosci*. 18:4008–4021.

Watson, D.F., J.W. Griffin, K.P. Fittro, and P.N. Hoffman. 1989. Phosphorylation-dependent immunoreactivity of neurofilaments increases during axonal maturation and beta,beta′-iminodipropionitrile intoxication. *J. Neurochem*. 53:1818–1829.

Willard, M., and C. Simon. 1983. Modulations of neurofilament axonal transport during the development of rabbit retinal ganglion cells. *Cell*. 35:551–559.

Wong, P.C., J. Marszalek, T.O. Crawford, Z. Xu, S.T. Hsieh, J.W. Griffin, and D.W. Cleveland. 1995. Increasing neurofilament subunit NF-M expression reduces axonal NF-H, inhibits radial growth, and results in neurofilamentous accumulation in motor neurons. *J. Cell Biol*. 130:1413–1422.

Xu, Z., J.R. Marszalek, M.K. Lee, P.C. Wong, J. Folmer, T.O. Crawford, S.T. Hsieh, J.W. Griffin, and D.W. Cleveland. 1996. Subunit composition of neurofilaments specifies axonal diameter. *J. Cell Biol*. 133:1061–1069.

Yabe, J.T., C. Jung, W.K Chan, and T.B. Shea. 2000. Phospho-dependent association of neurofilament proteins with kinesin in situ. *Cell Motil. Cytoskeleton*. 45:249–262.

Zhu, Q., S. Couillard-Despres, and J.P. Julien. 1997. Delayed maturation of regenerating myelinated axons in mice lacking neurofilaments. *Exp. Neurol*. 148:299–316.

Zhu, Q., M. Lindenbaum, F. Levavasseur, H. Jacomy, and J.P. Julien. 1998. Disruption of the NF-H gene increases axonal microtubule content and velocity of neurofilament transport: relief of axonopathy resulting from the toxin beta,beta′-iminodipropionitrile. *J. Cell Biol*. 143:183–193.